# Calcium Domains around Single and Clustered $IP_3$ Receptors and Their Modulation by Buffers

S. Rüdiger,[†] Ch. Nagaiah,[‡] G. Warnecke,[§] and J. W. Shuai[¶*]
[†]Institute of Physics, Humboldt-Universität zu Berlin, Berlin, Germany; [‡]Institute of Mathematics and Scientific Computing, University of Graz, Graz, Austria; [§]Institute for Analysis and Numerics, Otto-von-Guericke University, Magdeburg, Germany; and [¶]Department of Physics, and Institute of Theoretical Physics and Astrophysics, Xiamen University, China

ABSTRACT We study $Ca^{2+}$ release through single and clustered $IP_3$ receptor channels on the ER membrane under presence of buffer proteins. Our computational scheme couples reaction-diffusion equations and a Markovian channel model and allows our investigating the effects of buffer proteins on local calcium concentrations and channel gating. We find transient and stationary elevations of calcium concentrations around active channels and show how they determine release amplitude. Transient calcium domains occur after closing of isolated channels and constitute an important part of the channel's feedback. They cause repeated openings (bursts) and mediate increased release due to $Ca^{2+}$ buffering by immobile proteins. Stationary domains occur during prolonged activity of clustered channels, where the spatial proximity of $IP_3$Rs produces a distinct [$Ca^{2+}$] scale (0.5–10 $\mu$M), which is smaller than channel pore concentrations (>100 $\mu$M) but larger than transient levels. While immobile buffer affects transient levels only, mobile buffers in general reduce both transient and stationary domains, giving rise to $Ca^{2+}$ evacuation and biphasic modulation of release amplitude. Our findings explain recent experiments in oocytes and provide a general framework for the understanding of calcium signals.

## INTRODUCTION

The modulation of cytosolic calcium concentrations is a fundamental part of many cell-signaling networks. The calcium-rich endoplasmic reticulum (ER) releases $Ca^{2+}$ through inositol 1,4,5-trisphosphate receptor channels ($IP_3$ R) present in the ER membrane into the cytosol where concentrations of $Ca^{2+}$ are normally low (1). $IP_3$ Rs regulate $Ca^{2+}$ release in response to binding of $Ca^{2+}$ and $IP_3$ to receptor sites on the cytosolic side of the channels (2). Rebinding of liberated calcium to channels increases the open probability and provides a self-amplifying mechanism called calcium-induced calcium release. $Ca^{2+}$ released from a channel diffuses in the cytosol and increases the open probability of neighboring channels by binding to activating binding sites. Subsequently, increased $Ca^{2+}$ concentrations lead to closing of channels by binding of $Ca^{2+}$ to inhibiting sites.

An important aspect of coupling by diffusing $Ca^{2+}$ is the existence of multiple spatial scales and a related hierarchy of coupling strengths. At one end of the spatial spectrum are short openings of single channels called blips, where, in a self-loop, released $Ca^{2+}$ causes small close times and bursts of openings. Experimental observation of larger but still localized release events called puffs (3,4) indicates that functioning $IP_3$ R channels are grouped into clusters on the ER membrane containing, at most, a few tens of channels. The small number of channels and their proximity lead to stochastic but cooperative openings concerted by local diffusion of $Ca^{2+}$ and calcium-induced calcium release between adjacent channels (5,6). It has been argued that the different coupling strength between channels within the same cluster and those in different clusters is responsible for the hierarchical occurrence of puffs and cell-global release (7–9). According to this picture, global release occurs from clusters across the ER membrane at spacings of a few micrometers and requires synchronization of many clusters to form global oscillations and waves (4,10–12).

The complex role of calcium binding proteins (buffers) is a key issue in the modeling and understanding of diffusive coupling of $IP_3$ Rs. By binding and unbinding of calcium, buffers modify the equilibrium concentrations and are thus useful to experimentally change rest level concentrations of free calcium. However, the spatial and dynamical properties of coupled calcium/buffer systems are not well understood. Experiments with various exogenous buffers demonstrate the strong effect on the release that buffers can have (7,13,14). Dargan et al. (7,14) studied how the response of the $Ca^{2+}$ signal depends on the binding kinetics of $Ca^{2+}$ and buffers. The reaction to a stepwise increase of $IP_3$ was either a shortened release spike (for slow-binding buffer) or a prolonged release tail (for fast buffer).

The same authors also suggested that different buffers disrupt $Ca^{2+}$ feedback on different spatial scales. The influences of buffer can be distinguished following the hierarchy of the calcium system (i.e., influence on coupling between clusters, channels inside of a cluster, and self-feedback of a channel). In a modeling approach, Zeller et al. (8) and Falcke (15) studied the release from an array of clusters under the presence of buffers. On the other hand, the buffer effects on $Ca^{2+}$ released from a single deterministic channel were numerically and analytically discussed in the literature (16–19). Swillens et al. (5) investigated a stochastic $IP_3$ R

*Submitted August 31, 2009, and accepted for publication February 26, 2010.*

*Correspondence: jianweishuai@xmu.edu.cn

Editor: Arthur Sherman.



0006-3495/10/07/0003/10 $2.00

doi: 10.1016/j.bpj.2010.02.059

model within a cytosol-like environment and discussed the effect of various dye buffers on blip dynamics. A single channel in an immobile-buffer environment was studied numerically by Shuai et al. (20). The authors simulated the release dynamics of $IP_3$ Rs based on a stochastic nine-state model fitted to recent patch-clamp data (21). They found that reactivation of the channel depends strongly on immobile (or stationary) cytosolic $Ca^{2+}$ buffers. Immobile buffer delays the collapse of local $Ca^{2+}$ microdomains after each closure, when concentrations drop from $>100$ $\mu$M to rest levels of $<0.1$ $\mu$M.

We now extend this work by studying different buffers and combinations of buffers as well as by studying their effect on interaction of channels within a cluster. In this way, we close the gap between the available research on arrays of clusters and single channels. We identify the collapse of calcium domains as one of two important stages of intervention by buffers. While the transient lingering of free calcium ions after closing of channels dominates behavior of single channels, we find that release from clusters is determined by sustained calcium levels in the cluster area. A nontransient domain is maintained by repeated openings of channels in the cluster and can thus be regarded as a stationary (although fluctuating) attribute of release.

Mathematically, stationary domain calcium concentration is defined as a suitable average over time and over the individual channel domains in a cluster. We numerically determine its dependence on cluster geometry and buffers. In contrast to earlier work (8) we employ a three-dimensional, fully spatially resolved model of a cluster, that is, individual channels are located on the membrane with a certain separation from each other. This method allows us to show, for instance, that the level of stationary calcium falls with mobile buffer due to evacuation of calcium between channels and three-dimensional transport away from the cluster. Based on these results, we suggest that further analytical approaches should be built on cluster models with spatially separated channels rather than with one continuous source area (6,22,23).

## HYBRID STOCHASTIC AND DETERMINISTIC MODEL FOR CALCIUM DYNAMICS AND NUMERICAL METHODS

The model consists of partial differential equations for concentration fields and a Markovian description of discrete stochastic quantities. The concentration fields are the calcium concentration in the cytosol and the concentration of one or two buffers bound to calcium. Stochastic quantities are the discrete states of channel subunits, which determine the open/close states of each channel. We here adopt the nine-state model for the gating of subunits (21,24). Compared to the standard DeYoung-Keizer model (25) the nine-state model possesses an additional active state, which represents a conformational change of the subunit related to the channel opening (see Stochastic Model of Channel Gating in the Supporting Material).

The calcium concentration in the cytosol is determined by diffusion, the transport of calcium through the ER membrane, and the binding and unbinding of calcium to buffer molecules. In the cytosol, we consider the following types of buffers: exogenous mobile buffer with fast or slow reaction kinetics and a stationary buffer. Buffers are assumed to be distributed homogeneously at initial time. Parameters for the mobile and stationary types of buffers used for this work are listed in Table S1 in the Supporting Material.

The equations are either solved in a spherically symmetric domain (single channel) or in a cubelike domain. For the setup with a single $IP_3$ R channel that is located in the center of the cytosolic space, we use spherical symmetry to simplify the reaction-diffusion part of the model to a one-dimensional problem (20). The finite difference method proposed by Smith et al. (18) was used to solve the ensuing partial differential equations.

For release from several channels, the symmetric reduction is not possible. Instead, we use a cuboid of 5-$\mu$m height, where the bottom surface represents an idealized ER membrane of 8-$\mu$m side length (see Fig. 2 *A*). The bulk of the cube represents the cytosol of the cell, while boundary conditions at the bottom surface account for the membrane current consisting of channel, pump, and leak contributions. Channels are placed with a certain spatial separation $d$ on the surface. This method is distinct from the two-dimensional simulations in Zeller et al. (8), where all channels of a cluster were placed in a common source area. Our numerical method consists of coupled solvers for the deterministic set of partial differential equations and the stochastic equations. In view of the multiple space- and timescales, we employ a conforming finite element method for the spatial discretization and an adaptive linear implicit time-stepping for the deterministic part (26). The stochastic channel gating is incorporated by using the recently devised hybrid method (27). In (27) we established the equivalence of cuboid and spherical simulation results for single channels, which allowed us to use the reduced one-dimensional diffusion model with Markovian channel dynamics to save computation time for our current work. For a more detailed description of model equations and numerical methods, see section S1 and S2 of the Supporting Material.

## RESULTS FOR SINGLE CHANNEL DYNAMICS

For an isolated channel, we will first discuss the case of a single buffer, either immobile or mobile and then extend the discussion to the case of two buffers acting simultaneously. Shuai et al. (20) studied the dynamics of a single channel in the presence of stationary buffer and found a strongly shortened mean close time with almost unchanged mean open time, and thus an overall increase of open

probability at large buffer concentrations (*squares* in Fig. 1, *A–C*). This effect results from the fact that stationary buffer extends the lifetime of $Ca^{2+}$ domains around active channels beyond the time when the channel has already closed (*dotted line* in Fig. 1 *E*). The buffer-bound $Ca^{2+}$ will be released relatively slowly after the channel has closed and may subsequently bind to the channel and open it again, leading to bursts of channel openings and closings.

## Mobile buffer alone has little effect on single channel dynamics

We next consider mobile buffers either with slow reaction kinetics (representing EGTA) or fast reaction kinetics (BAPTA). The results are included in Fig. 1, *A–C* (*up-triangles* for BAPTA and *down-triangles* for EGTA). In contrast to the case of immobile buffer, increasing mobile buffer concentration has little effect on the single channel dynamics.

To elucidate the different action of mobile and immobile buffer on channel closing, we made deterministic simulations with a channel opening for 6 ms, which is the mean open time of a single channel (Fig. 1 *B*). Fig. 1, *D* and *E*, shows the local $Ca^{2+}$ concentration at the channel pore during and after channel openings with different concentrations of BAPTA and EGTA. Fig. 1, *D* and *E*, demonstrates that the decay rate of the free $Ca^{2+}$ concentration at the channel pore increases as a function of increasing concentration of mobile buffer. This occurs because mobile buffers bind the released free $Ca^{2+}$ ions at the channel pore and act as a shuttle to carry the $Ca^{2+}$ ions away from the channel pore. BAPTA is a faster binding/unbinding buffer than EGTA, thus a larger decay rate can be observed for BAPTA than EGTA at the same buffer concentration. The fast decay of $[Ca^{2+}]$ after channel closing explains the ineffectiveness of mobile buffer in reopening of channels. For comparison, the local $Ca^{2+}$ concentration at the channel pore with the 800 $\mu$M immobile buffer is also plotted in Fig. 1 *E*, showing the opposing effect on $Ca^{2+}$ decay after channel closing discussed above.

In Fig. 1, *A–C*, blip dynamics are characterized for $IP_3$ concentrations at 0.2 and 1.0 $\mu$M. Generally, a larger open probability with a smaller close time is obtained with increased $IP_3$ concentration.

## Mobile buffer competes with stationary buffer and reduces opening probability in two-buffer setups

Now we discuss the effects of EGTA and BAPTA on single channel dynamics in the presence of stationary buffer. The immobile buffer is fixed at 800 $\mu$M in the system. With increasing mobile buffer concentration, the mean close time increases strongly (data shown in Fig. S1 *A*) with a slightly increased mean open time (Fig. S1 *B*), resulting in a decrease of the open fraction (Fig. S1 *C*). The 800-$\mu$M

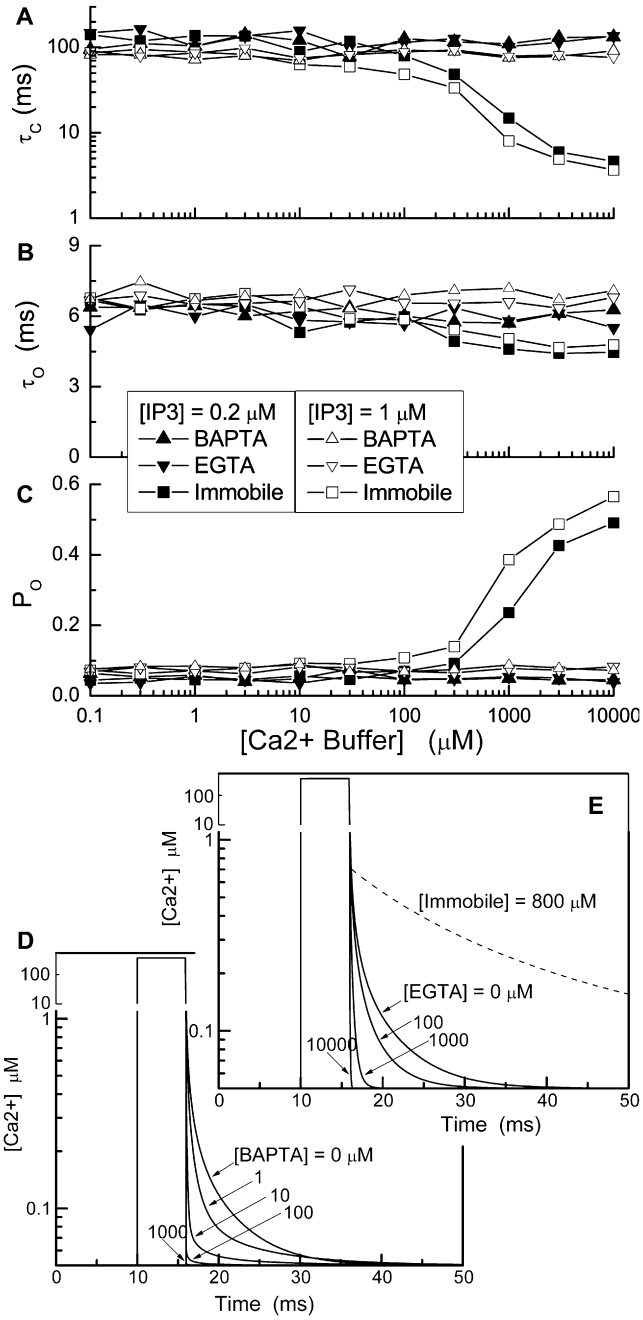


FIGURE 1 The blip dynamics as a function of the concentration of an immobile buffer or a mobile buffer for $IP_3$ concentrations of 0.2 and 1.0 $\mu$M. (*A*) Mean close time. (*B*) Mean open time. (*C*) Open probability. The effects of mobile buffers on the decay rate of the free $Ca^{2+}$ concentration at the channel pore are shown in panels *D* and *E*. The $Ca^{2+}$ concentration at the channel pore is plotted as a function of time with the channel held open for 6 ms. (*D*) BAPTA at concentrations of 0, 1, 10, 100, and 1000 $\mu$M and (*E*) with EGTA at concentrations of 0, 100, 1000, and 10,000 $\mu$M. The dashed line shows the evolution under the presence of immobile buffer.

immobile buffer will cause a slow decay of $Ca^{2+}$ concentration after channel closing. However, mobile buffer acts as a shuttle to carry the $Ca^{2+}$ ions away from the channel pore. The free $Ca^{2+}$ concentration will diminish to its

resting-state level within a shorter time, resulting in a smaller chance for the channel to reopen. Thus, the higher concentration of mobile buffer causes a longer mean close time and a smaller open probability.

Fig. S1 also shows that the mean open time of a single channel is insensitive to both EGTA and BAPTA buffers. However, the mean close time and the open probability show different behaviors for the two types of mobile buffers in the range of 1–1000 $\mu$M. From Fig. 1, *D* and *E*, it can be seen that the shuttle effect on free calcium after channel closing for 10-$\mu$M BAPTA is similar to that for 1000-$\mu$M EGTA. Thus, the open probability of the channel with 3-$\mu$M BAPTA is similar to that with 1000-$\mu$M EGTA (Fig. S1 *C*). The differences for both the mean close time and the open probability become less significant for EGTA and BAPTA buffers at large concentrations. The shuttle effect for mobile buffer at large concentration is so strong that the slow decay caused by the immobile buffer will no longer exist, no matter if the mobile buffer is fast or slow. The $IP_3$ R dynamics in this case reaches the limiting situation of absence of buffers. Indeed, the open probability of ~0.05 with mean open time close to 6 ms and mean close time close to 100 ms is similar to the result given in Fig. 1. Our results have been summarized qualitatively in columns 2 and 3 of Table 1.

We have also studied the effects of changing the diffusion coefficient and the $IP_3$ concentration on single channel dynamics. A discussion is included in Single-Channel Simulations in the Supporting Material and in Fig. S2 and Fig. S3.

## MULTICHANNEL SIMULATIONS

To test the significance of our single-channel results, we simulated the release dynamics of a cluster with nine channels using the hybrid simulation method. Channels were arranged in a $3 \times 3$ grid with grid distances $d$ from 15 to 1000 nm (Fig. 2 *A*). Generally, we simulated for a total of 11 s and recorded the number of open and inhibited channels as well as the calcium and buffer distributions at the membrane. In the simulations presented below, the channels were stimulated by a step increase of [IP3] from 0.01 to 0.2 $\mu$M at time $t = 1.0$ s, unless stated otherwise. Channels opened stochastically and cooperatively so that the random opening of a first channel normally triggered opening of further channels. Fig. 2 *B* shows a representative evolution of the free $Ca^{2+}$ concentration at the pores of three selected channels for $d = 30$ nm (no buffer). An open channel can be identified by a $Ca^{2+}$ concentration at the pore, $[Ca^{2+}]_{pore}$, that exceeds 100 $\mu$M. On the other hand, if a channel is closed, but one or more other channels are open, $[Ca^{2+}]_{pore}$ falls to ~10 $\mu$M, even if a channel is closed very briefly. If all channels are closed sufficiently long, $[Ca^{2+}]_{pore}$ decreases to the rest level of 0.05 $\mu$M.

As before in the case of a single channel, the level of $Ca^{2+}$ concentration at the mouth of a closed channel determines the probability to open again and thus to undergo bursts of repeated openings and closings. Because of its role as a mediator of buffer effects on channel gating, we will refer to the suitably averaged, local concentration of $Ca^{2+}$ as cluster domain concentration. We will first discuss the case of immobile buffer and mobile buffer separately, and then study the case of two combined buffers.

**TABLE 1 Qualitative dependence of calcium concentrations and open probabilities on three types of buffer**

| Buffer | Isolated channel | | Clustered channels | |
|---|---|---|---|---|
| | Transient $[Ca^{2+}]$ | $P_o$ | Stationary $[Ca^{2+}]$ | $P_o$ |
| Immobile | ↑ ↑ | ↑ | → | → |
| Fast | ↓ ↓ | ↓* | ↓ | ↑† ↓ |
| Slow | ↓ | ↓* | → | → |

Up/down arrows indicate whether a quantity increases or decreases, respectively.

*Here we assumed an environment of immobile buffer, where addition of mobile buffer eliminates transient domains and decreases open probabilities.

†The increase of open probability only occurs under certain conditions. For instance, for very closely packed clusters without additional buffer, we found strong inhibition. An increase of fast buffer concentration then decreases $[Ca^{2+}]_{dom}$ below the dissociation constant of inhibition. As a result, a reduction of inhibition occurs and thus the open probability can increase (see Fig. 5 *A*). For larger channel distances, domain $Ca^{2+}$ values may already be below $K_{inh}$ before addition of buffer and the dominant effect is a decrease in activation (compare Fig. 6).

## Open probability is independent of stationary buffer for clusters of channels

We calculated mean quantities as averages for the time interval from 1 s to 11 s using output time steps of 1 ms, to characterize the long time gating behavior. We found above that for a single channel the open probability is close to 5% if no buffer is present. The open probability strongly increases with increasing amounts of stationary buffer (see Fig. 1). Surprisingly, for the nine-channel setup, no clear dependence of the open probability on immobile buffer concentration was found for channel distances of up to 120 nm (Fig. 3). Linear fits show that $P_o$ is approximately constant, for instance at ~0.2 for $d = 30$ nm. $P_o$ increases with $d$, reaches a maximum of ~0.3 at intermediate channel distances of 120 nm, and decreases again for larger channel distances.

In contrast to small and intermediate $d$, for channel distances of 1000 nm, the open probability increases with the buffer concentration (Fig. 3) for $[B_{imm}] > 80$ $\mu$M. We note that for large distances, the coupling of channels is small, so that one recovers the case of individual channels in which the open probability increases strongly with the buffer concentration.

To elucidate the different behavior of single and clustered channels we will now discuss the concentration of free $Ca^{2+}$ in the cluster area and its modulation by buffer. Because only the free calcium concentration at the binding site, $[Ca^{2+}]_{pore}$, enters the gating behavior of a channel, we evaluated the calcium concentrations at each of the nine channel's pores. The distribution of channel pore concentrations at all times and all channels is shown in Fig. 4 (for all distribution,

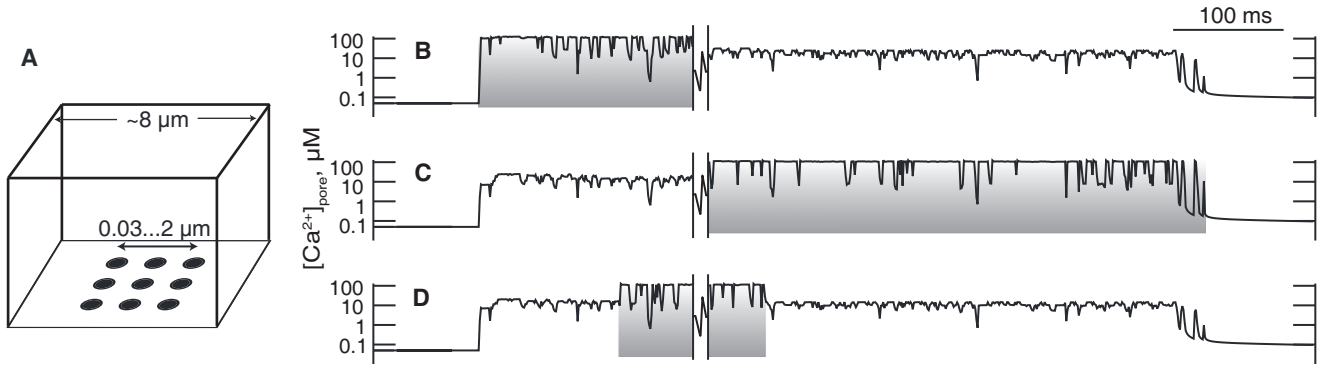


FIGURE 2 (*A*) Schematic plot of the computational model for a cluster of nine channels. The lower surface represents the ER membrane. (*B–D*) Evolution of free calcium concentration at the channel center for three representative channels. In this simulation, $d = 30$ nm, and no buffer was used. Release bursts are indicated by the underlaid shaded boxes. If a channel is open, the $Ca^{2+}$ concentration reaches >100 $\mu$M. However, if a channel is closed but other channels in the cluster are open, the concentration falls to ~10 $\mu$M within <1 ms, approximately independent on the distance from an active channel.

we excluded instances of $[Ca^{2+}]_{pore} < 0.051$ $\mu$M). The plots represent the overall distribution (Fig. 4 *A*), the distribution for times when all channels are closed (Fig. 4 *B*), and the distribution of values at closed channels in the presence of open channels (Fig. 4 *C*). In the overall distribution (Fig. 4 *A*) for control (no buffer), three qualitatively different contributions were found. At ~100 $\mu$M we identify the local concentration at open state (peak 1). A second contribution occurs between 0.05 and 0.1 $\mu$M (peak 2). As can be concluded from comparison with Fig. 4 *B*, this maximum corresponds to a transient calcium concentration, which relaxes to rest level after all channels have closed. A third contribution at ~10 $\mu$M (peak 3) represents channels that are closed, but where different channels in the cluster are open (compare Fig. 4 *C*).

Now we turn to the case of immobile buffer. The largest difference to the prior case occurs in plot Fig. 4 *B*, which shows the distributions of $[Ca^{2+}]_{pore}$ at times when all channels have closed. For immobile buffer, a much higher presence of calcium was found. This results from the effect of immobile buffer, as discussed in Results for Single Channel Dynamics—namely that it delays the relaxation to rest state and thus, strongly increases the transient calcium. As the open probability in clusters is insensitive to immobile buffers, it follows that $P_o$ cannot depend on the amplitude of transient domains. On the other hand, the distribution in Fig. 4 *C*, which corresponds to a sustained (or stationary) calcium elevation, is not changed significantly compared to the control case. Therefore, $P_o$ may still be changed if the amplitude of stationary domains is modulated (see below). We tentatively conclude from this consideration that the distributions shown in Fig. 4 *C*, but not those in Fig. 4 *B*, determine the release amplitude in clusters.

## Adjacent active channels determine local $Ca^{2+}$ concentration at closed channels

The persistence of the calcium distribution shown in Fig. 4 *C* and its narrow base under addition of immobile buffer suggests that we further consider the average concentration of this distribution. We will show that this average calcium value is strongly related to the changes of open probability for varying channel distance $d$ and concentration of fast mobile buffer. The average thus characterizes the relevant calcium concentration of the cluster.

If $c_i(t)$ is the $Ca^{2+}$ concentration at the mouth of channel $i$, ($i = 1,\ldots, N = 9$) at time $t$ ($t$ from $t_0 = 1,\ldots t_1 = 11s$) and $o_i(t)$ is the open or close state of the channel (i.e., $o_i = 0$, closed, or 1, open), we define

$$\left[Ca^{2+}\right]_{dom} = \sum_i \frac{1}{NT_i} \int_{t_0}^{t_1} c_i(t)(1 - o_i(t))\ \mathrm{sgn}(N_o(t))dt, \quad (1)$$

where

$$T_i = \int_{t_0}^{t_1} (1 - o_i(t))\ \mathrm{sgn}(N_o(t))dt$$

is the total time that the $i^{th}$ channel is closed but at least one other channel is open, where

$$N_o(t) = \sum_i o_i(t)$$

is the number of open channels at time $t$ and sgn($x$) gives +1 if $x$ is positive and 0 if $x = 0$. The cluster domain concentration $[Ca^{2+}]_{dom}$ is the average concentration that a channel is subjected to if it is closed but the cluster is active.

$[Ca^{2+}]_{dom}$ for different channel distances and different $[B_{imm}]$ is shown in Fig. 3 *B*. First, we argue that the $[Ca^{2+}]_{dom}$ value is constant with increasing amounts of immobile buffer. In contrast, the average, that is taken after closing of all channels, increases as it does in the single-channel case (data not shown). Furthermore, we found that $[Ca^{2+}]_{dom}$ values decrease with the channel distance. It is ~10 $\mu$M at 30 nm, 5 $\mu$M for 120 nm, and as small as 0.5 $\mu$M at 1000 nm. Fig. 3, *A* and *B*, indicates that the domain

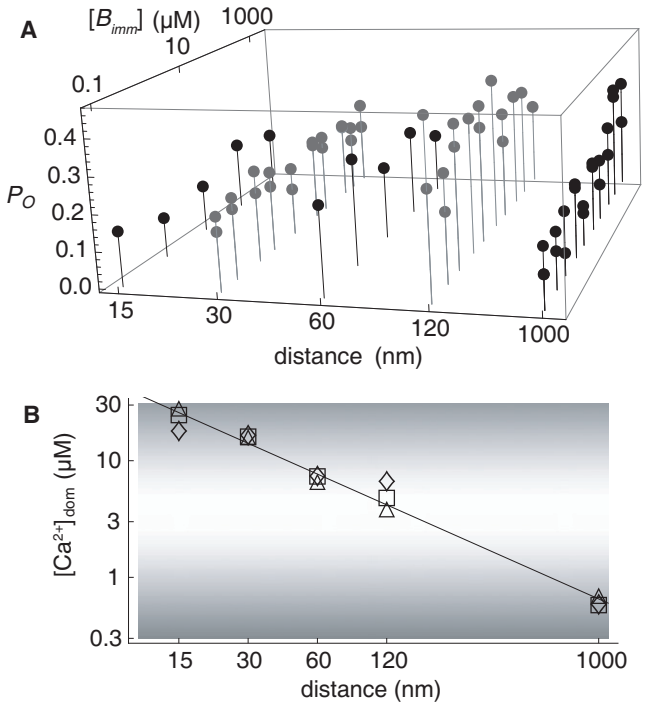


FIGURE 3 (*A*) The mean open fraction depends on the distance $d$ between channels but it does not depend on the amount of immobile buffer (except for large channel distance $d = 1000$ nm). For each pair of parameters ($d$,[$B_{imm}$]), one or two simulations of 10 s were evaluated and results are represented by circles attached to the pins. (*B*) The stationary concentration $[Ca^{2+}]_{dom}$ does not vary with [$B_{imm}$] (◇, 0.08 $\mu$M, □, 80 $\mu$M, and △, 8000 $\mu$M), but strongly decreases with channel distance $d$. The reduction of $[Ca^{2+}]_{dom}$ with cluster size results in larger probability of a subunit to be in the active state $X_{ACT}$ (*open horizontal area*) for intermediate distances at ~120 nm and small probability for very small and very large distances (*dark shaded areas*). The shading scale has been obtained from Eq. 2 with $K_{act} = 0.8$ $\mu$M and $K_{inh} = 16$ $\mu$M. (*Solid line*) Fitted calcium domain as a function of distance. The cross-point of the solid line with the central open area is at ~200 nm.

calcium concentration determines the open probability. It remains to us to consider why $P_o$ exhibits a maximum at intermediate channel distances. We first note that domain calcium values for intermediate $d$ are close to the dissociation constants of inhibition ($d_2 = 16$ $\mu$M) and activation ($d_5 = 0.8$ $\mu$M). We therefore suggest that the open probability should be largest if the domain calcium concentration $[Ca^{2+}]_{dom}$ is ~2–5 $\mu$M (large activation and small inhibition). To make this observation more precise, we can estimate the probability of a subunit to be activated and not inhibited (i.e., the subunit is in the state $X_{ACT}$) as the product of three factors

$$P_{s.u.} = \frac{a_0}{a_0 + b_0} \frac{[Ca^{2+}]_{dom}}{K_{act} + [Ca^{2+}]_{dom}} \left(1 - \frac{[Ca^{2+}]_{dom}}{K_{inh} + [Ca^{2+}]_{dom}}\right). \quad (2)$$

The second and third factors determine the probability for a subunit to be active and not inhibited, respectively, while the first factor calculates the fraction of time spent in the active state compared to the state $X_{110}$ ($a_0$ and $b_0$ are the on- and off-rates of the transition from $X_{110}$ to the active state). $K_{act,\ inh}$ values are dissociation constants of activating and inhibiting binding processes. $P_{s.u.}([Ca^{2+}]_{dom})$ has been gray-shaded in Fig. 3 *B* under the assumption of large $IP_3$ concentration, showing that largest activation probabilities occur for ~200-nm channel distance, which is the cross-point of the open white area and the solid line of the linearly fitted domain calcium as a function of distance. This observation is consistent with the larger open probability for the channel geometry of 120 nm distance compared to 30 nm and 1000 nm smaller and larger distances.

## Mobile buffer affects $Ca^{2+}$ release in two regimes

A strong impact of buffer was found for the case of mobile buffer with fast reaction kinetics (corresponding to BAPTA). The open probability for a setup with 30-nm channel distance is shown in Fig. 5 *A*. For small buffer concentration,

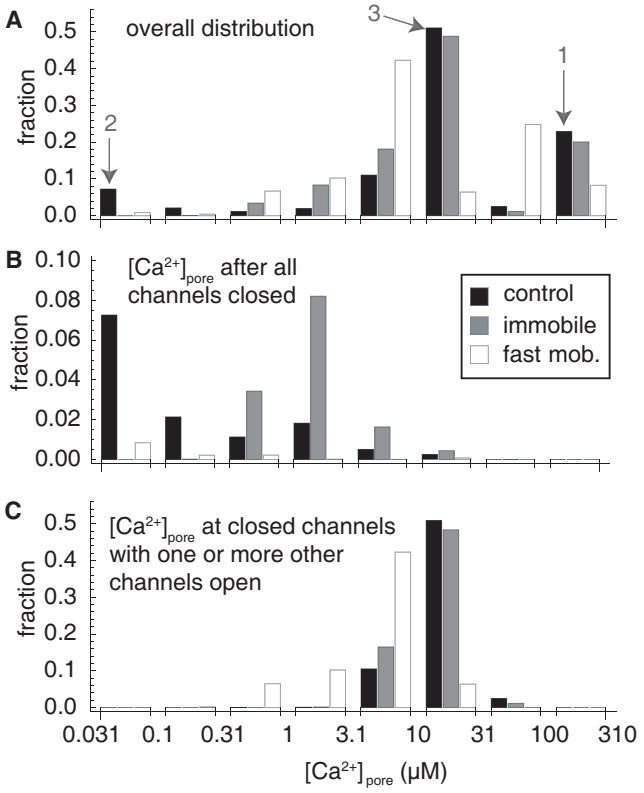


FIGURE 4 Distribution of channel mouth $Ca^{2+}$ concentrations for runs without and with two different buffers. The three plots show the overall distributions (*A*), the distributions of $Ca^{2+}$ concentrations when all channels are closed (*B*), and the distributions of $Ca^{2+}$ concentration at a channel when it is closed, but other channels in the cluster are open (*C*). Each bar corresponds to one simulation over 10 s for control, 800 $\mu$M stationary buffer, or 800 $\mu$M fast mobile buffer. We have neglected instances where $[Ca^{2+}]_{pore} < 0.051$ $\mu$M. Numbers at arrows denote the order by which peaks are mentioned in the main text.

the open probability is close to the value of 0.2, which was found before for the case of stationary buffer or without buffer. However, with increasing buffer concentration the open probability increases to levels >0.3 at 2000 $\mu$M concentration. If the buffer concentration is further increased, the open probability decreases strongly to 0.1. In effect, there is a distinct maximum of the open probability for buffer concentrations at ~2000 $\mu$M. For EGTA (slow mobile buffer), no significant effect was found.

To elucidate the behavior for BAPTA, we have plotted the cluster domain concentration $[Ca^{2+}]_{dom}$ and the fraction of inhibited channels in Fig. 5 *B*. For increasing amounts of BAPTA, $[Ca^{2+}]_{dom}$ decreases from ~16 $\mu$M to 0.1 $\mu$M. This effect can also be seen from Fig. 4 *C*, where for fast mobile buffer the distribution moves to the left compared to the other two cases. Accordingly, only for small amounts of mobile buffer are many channels inhibited. For larger buffer concentration, $[Ca^{2+}]_{dom}$ and inhibition are reduced resulting in a large $P_o$. For amounts of buffer beyond 4 mM, $[Ca^{2+}]_{dom}$ is becoming even smaller and loses its capacity to stimulate frequent openings of neighboring channels. This corresponds to a strong isolation of channels, so that for large mobile buffer concentration the open probability of individual channels, at ~5%, is recovered.

To quantify this argument we will now make an estimate of the open probability. We first observe that the logarithm of the domain calcium concentration assumes an almost linear behavior if plotted against the buffer concentration in linear scale (Fig. 5 *B*, *inset*). We therefore approximate

$$\left[Ca^{2+}\right]_{dom} = C_0 e^{-\alpha B_m}, \quad (3)$$

where $B_m$ denotes the total amount of mobile buffer, $C_0 = 16$ $\mu$M is the estimated domain concentration at $B_m = 0$, and $\alpha$ is a fitting constant obtained (as shown by the *straight line* in Fig. 5 *B*, *inset*).

Using the argument of the previous section, the open probability of a channel is then obtained from the fact that three or four subunits should be in the active state,

$$P_o = P_{s.u.}^4 + 4P_{s.u.}^3(1 - P_{s.u.}), \quad (4)$$

where $P_{s.u.}$ is given by Eqs. 2 and 3. This expression has been evaluated to the solid line in Fig. 5 *A*, clearly showing qualitative agreement with the numerical data points and proving the significance of the domain calcium concentrations for the open probability.

The decrease of domain calcium originates from the narrower microdomains around open channels. This can be clearly seen in Fig. S4 *C*, which shows that $[Ca^{2+}]$ is almost at rest level at the location of closed channels for large $B_m$. We therefore conclude that addition of fast mobile buffer strongly reduces the coupling of channels within a cluster by diffusing calcium. Note that for large amounts of BAPTA the $[Ca^{2+}]_{dom}$ reduction down to 0.1 $\mu$M can be even stronger than the spatial decoupling by placing the channels

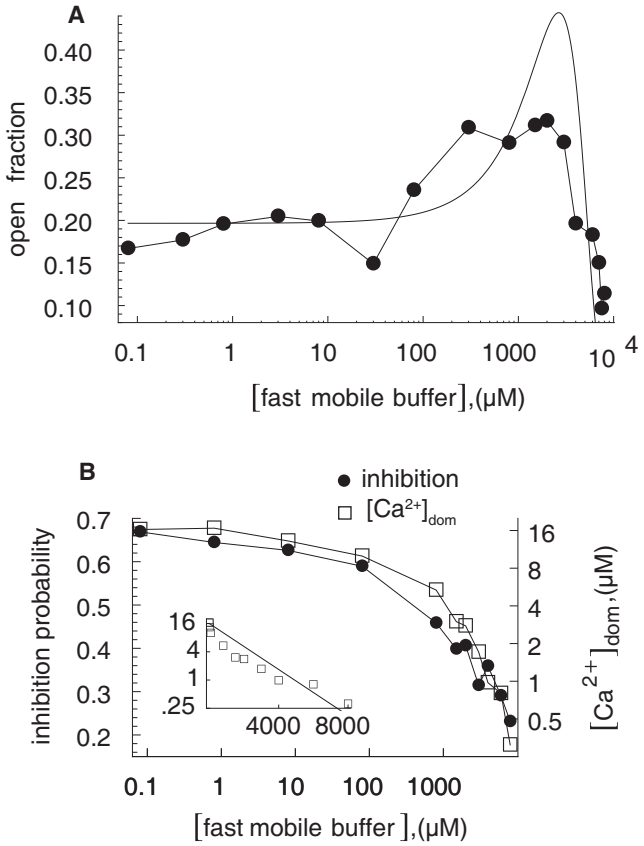


FIGURE 5 Simulations with various amounts of mobile buffer with fast reaction kinetics (BAPTA) and grid constant $d = 30$ nm. (*A*) Open probability (to reduce fluctuations we have averaged over 20 s for each data point). The smooth curve shows the analytical approximation using Eq. 4 and $K_{act} = 0.8$ $\mu$M, $K_{inh} = 16$ $\mu$M. (*B*) Fraction of inhibited channels and the cluster domain calcium. (*Inset*) Exponential fitting of the cluster domain concentration ($\alpha = 5.64 \times 10^{-4}$ $\mu M^{-1}$).

1 $\mu$m apart, in which case $[Ca^{2+}]_{dom}$ values are close to 0.5 $\mu$M. Our results for mobile buffer have been summarized in columns four and five in Table 1.

## Immobile buffer is also ineffective in two-buffer environments of clustered channels

The contradiction between the effects of immobile buffer in mono- and multichannel setups motivated us to also consider the case of two simultaneous buffers for clusters. Specifically, we now discuss cluster simulations for immobile buffer combined with fast mobile buffer. The decrease of $[Ca^{2+}]_{dom}$ for fast mobile buffer that we found can be interpreted as follows: Fast mobile buffer binds released calcium and shuttles it away, thus reducing the size of the calcium domains around each open channel (Fig. S4 *C*). For very large buffer concentration this corresponds in effect to a growing spatial isolation of channels, similar to a very large distance $d$ of channels. Further, for isolated channels we had seen earlier that immobile buffer

has a strong impact on the open probability by delayed release of bound calcium. It is therefore possible that immobile buffer counteracts the effect of fast buffer and increases $P_o$ by a mechanism similar to the one for an isolated channel. We ask now if there is a significant change of $P_o$ for immobile buffer in the presence of large quantities of fast mobile buffer.

The open probability for various mobile buffer concentrations and zero or 8000 $\mu$M immobile buffer is shown in Fig. 6 (see Two-Buffer Simulations for Multichannel Setup in the Supporting Material for information on the simulation method based on larger pores). It is apparent that the open probability decreases for large mobile buffer concentrations, but does not depend on the amount of immobile buffer. This result shows that immobile buffer does not modify cluster release amplitude even in the presence of large amounts of mobile buffer. This occurs because, similar to the mechanism for the single-channel with two buffers, mobile buffer rapidly destroys local calcium domains after a channel has closed. Thus, even in the presence of high quantities of immobile buffer, the probability to reopen is not modified.

Fig. 6 also shows the experimental dependence of calcium release amplitude measured by Dargan and Parker (7). They have estimated the maximal fluorescence level $V_{max}$ for saturating levels of $IP_3$ and various amounts of BAPTA buffer (*solid diamonds*). $V_{max}$, which is an indirect measure of calcium release, increases slightly for small levels of BAPTA (compared to the control case), but decreases sharply for values of 100 $\mu$M and above. While the relatively low spatial resolution of experimental measurements does not allow the estimation of release amplitudes of individual channels or clusters, we here suggest that the lower overall amplitude is due to the decrease of open channel numbers for each cluster. In that respect, the good agreement with our simulation results shows that the intervention of BAPTA between the channels of a single cluster discussed in this article is sufficient to explain the experimentally observed decrease of global calcium release. This finding demonstrates the significance of our analysis for whole-cell release properties.

In contrast to the simulations for a channel distance of 120 nm, the 30-nm case exhibits a decrease in calcium release at much higher values (compare Fig. 5). This comparison suggests that the actual channel distance in clusters of *Xenopus* oocytes is closer to 120 nm than to 30 nm. It also implies that the cluster typically has a relatively large size, which has been first proposed in Shuai et al. (28) and confirmed experimentally in Demuro and Parker (29).

We finally note that our results are independent of $IP_3$ concentration. The inset in Fig. 6 shows that for $IP_3$ concentration increased to 1.0 $\mu$M, the reduction of $P_o$ occurs at approximately similar values to BAPTA concentration. This finding supports our interpretation that the effects of buffer on calcium release are mediated directly through the cluster domain calcium concentration.

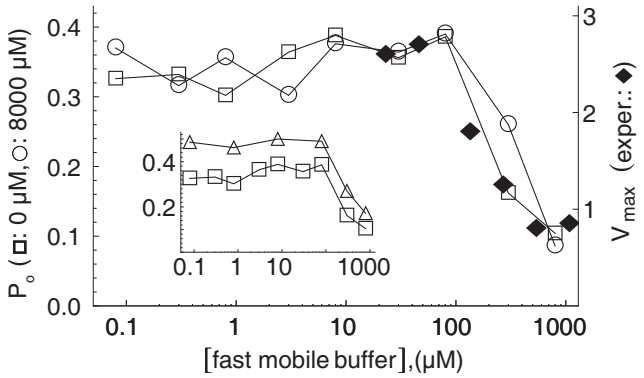


FIGURE 6 The open probability for various amounts of fast mobile and stationary buffer in a setup with nine channels and 120-nm channel distance (*open symbols*). Each data point is an average over 50 s. These results were obtained using the large-pore method under the presence of fast mobile buffer and zero (□) or 8000 $\mu$M (○) stationary buffer. For comparison we have plotted the amplitude of $Ca^{2+}$ release obtained in experiments on *Xenopus* oocytes (see Fig. 4 *B* in (7)). (◆) Peak fluorescence level $V_{max}$. The right axis has been scaled to match the values of simulations and experiments for vanishing amount of mobile buffer. (*Inset*) $P_o$ for two different $IP_3$ concentrations of 0.2 (□) and 1.0 $\mu$M (△).

## CONCLUSIONS

Our simulations have shown a strong dependence of calcium release on buffer. For a single channel we found that its open fraction increases and the mean closed time decreases with the concentration of an immobile buffer, whereas mobile buffer alone does not change release dynamics. The increase of open probability with immobile buffer results from the slower decay of $[Ca^{2+}]$ after channel closing, which is not observed for mobile buffer. A different picture emerges if one considers two buffers simultaneously. We found that a sufficiently large amount of mobile buffer counteracts the release-increasing effect of immobile buffer and reduces open probability. Mobile buffer takes up calcium from the stationary buffer after the channel has closed and shuttles it away. Therefore, the delaying effect of immobile buffer is lost. This effect is observed both for fast and slow mobile buffer; however, due to the smaller reaction rate, the effect is much smaller for slow buffer (Table 1, second and third column).

Because of the strong effect of immobile buffer for a single channel it came as a surprise that it is ineffective in clusters of channels. Here we found no influence of immobile buffer on the open probability. The reason is the typically large concentration of calcium in the cluster area as a whole. Because on average ~20% of the channels are open for $IP_3$ concentrations of 0.2 $\mu$M without additional buffer (i.e., there are always approximately two of nine channels open), the released calcium keeps the concentration relatively high at ~10 $\mu$M. This concentration is much higher than the typical calcium concentration after closing of an isolated channel (<0.7 $\mu$M, see Fig. 1 *E*), and therefore, in a cluster of channels, the transient calcium is of negligible

importance compared to the calcium arriving from neighboring channels.

We also found that, in contrast to the single channel simulations, fast mobile buffer has a strong effect on multichannel dynamics even if used in a one-buffer environment. We therefore obtain a reversal of the findings for a single channel. Note that the inefficiency of immobile buffer in the multichannel case was even found for two simultaneously acting buffers. Based on these results, one can neglect the immobile buffer, at least in the case of sustained release for large $IP_3$ concentration, when at least one channel stays open.

To further elucidate the contrasting pictures for single and clustered channels we have calculated the average pore concentration for channels at those times, at which they are closed, provided that different channels in the cluster are open. This concentration, which we call cluster domain concentration ($[Ca^{2+}]_{dom}$), is a stationary quantity during sustained release periods and strongly depends on the type and amount of buffer. Particularly, it decreases drastically with higher concentrations of fast mobile buffer, but does not change with immobile buffer. There is therefore a clear correspondence of this relation to the relation of buffer with open probability (see Table 1). This also implies that buffers predominantly affect the open probability through tuning of interaction of channels, and not, as suggested by the single channel results, self-feedback. Our work thus supports the conjecture that fast mobile buffer (BAPTA) acts on communication between $IP_3$ Rs within a cluster (7).

Our results suggest that the spatial separation of channels within a cluster cannot be neglected. This finding contradicts earlier research, which concluded that all channels of a cluster can be subsumed in one source area. Swillens et al. (22) do not find differences in stochastic simulations of clusters when they considered spatial separation of 12 nm or channels homogeneously distributed in a virtual domain. The finding can be understood from the fact that domain calcium values for 12 nm should be larger than any dissociation constant and thus no difference in open probability to the virtual-domain approach appears. However, newer theoretical and experimental work suggests a much larger distance of channels and a cluster diameter of a few hundred nanometers (28,29). Our investigation indicates that in a large geometry domain, calcium concentrations are close to the dissociation constants of the subunit's binding sites. Therefore, the virtual domain cannot adequately describe the local calcium concentrations and its feedback on the channel gating.

We briefly compare the effects of buffer in our analysis to those found in experiments. A feature of the effect of BAPTA in our simulations is that with moderate amounts of BAPTA, inhibition of channels is reduced more strongly than activation. Because repeated spiking of calcium release is thought to incorporate inhibition of channels, we expect that for moderate amounts of BAPTA the decaying part of an oscillation, but not its activation, is eradicated. This behavior was indeed found in the experiments by Rintoul and Baimbridge (13). There it was shown that for cells without treatment, baseline spiking can be triggered. However, for moderate amounts of BAPTA, no spiking can be observed, while >40% of the cells respond with an active, monophasic state. In addition, we found that for large amounts of BAPTA, activation is also depressed. This finding provides an understanding of an important aspect in the experiments of Dargan et al. (14). The reduction of fluorescence peak level found there is reflected in our dependence of open fraction on BAPTA concentration (see Fig. 6).

We finally emphasize that, as suggested by Table 1, most of our results are consequences of the geometry of channel positioning, transport of $Ca^{2+}$, and the action of buffer rather than the single channel kinetic model. Our single cluster model thus captures essential processes during cell global calcium release independent of the concrete $IP_3$ R model. For instance, activation of channels by $Ca^{2+}$ from neighboring open channels is a universal property of kinetic gating models with dissociation constant ~1 $\mu$M (30). Generally, for additional fast mobile buffer we then confirm the experimentally observed existence of a regime of reduced open probability (Fig. 5 *A* and Fig. 6). However, in our kinetic model, inhibition of channels requires the transition from the open to the closed state and is therefore dominated by domain calcium concentrations. This implies that intermediate concentrations of fast buffers can cause an increase of release amplitude by reduced inhibition (compare Fig. 5 *A*). In different models, as for instance the standard DeYoung-Keizer model (25), inhibition can occur in the open state of a channel, in which case the latter effect is not occurring and the up-arrow in $P_o$ for fast buffer in Table 1 can disappear. Our analysis, in combination with experimental studies, may thus provide further cues for the verification of detailed and specific gating models.

## SUPPORTING MATERIAL

Three additional sections with six equations, two tables, and four figures are available at http://www.biophysj.org/biophysj/supplemental/S0006-3495(10)00425-X.

This work was supported by grant No. FA 350/6-1 of the Deutsche Forschungsgemeinschaft within the priority program No. SPP 1095, "Analysis, Modeling, and Simulation of Multiscale Problems". J.W.S. acknowledges support from the National Science Foundation of China under grant No. 10775114 and National Institutes of Health grant No. 2R01GM065830-06A1.

## REFERENCES

1. Berridge, M. J., M. D. Bootman, and H. L. Roderick. 2003. Calcium signaling: dynamics, homeostasis and remodeling. *Nat. Rev. Mol. Cell Biol.* 4:517–529.
2. Foskett, J. K., C. White, …, D. O. Mak. 2007. Inositol trisphosphate receptor $Ca^{2+}$ release channels. *Physiol. Rev.* 87:593–658.

3. Parker, I., and Y. Yao. 1996. $Ca^{2+}$ transients associated with openings of inositol trisphosphate-gated channels in *Xenopus* oocytes. *J. Physiol.* 491:663–668.
4. Marchant, J. S., and I. Parker. 2001. Role of elementary $Ca^{2+}$ puffs in generating repetitive $Ca^{2+}$ oscillations. *EMBO J.* 20:65–76.
5. Swillens, S., P. Champeil, …, G. Dupont. 1998. Stochastic simulation of a single inositol 1,4,5-trisphosphate-sensitive $Ca^{2+}$ channel reveals repetitive openings during 'blip-like' $Ca^{2+}$ transients. *Cell Calcium.* 23:291–302.
6. Shuai, J. W., and P. Jung. 2002. Stochastic properties of $Ca^{2+}$ release of inositol 1,4,5-trisphosphate receptor clusters. *Biophys. J.* 83:87–97.
7. Dargan, S. L., and I. Parker. 2003. Buffer kinetics shape the spatiotemporal patterns of $IP_3$-evoked $Ca^{2+}$ signals. *J. Physiol.* 553:775–788.
8. Zeller, S., S. Rüdiger, …, M. Falcke. 2009. Modeling of the modulation by buffers of $Ca^{2+}$ release through clusters of $IP_3$ receptors. *Biophys. J.* 97:992–1002.
9. Rüdiger, S., and L. Schimansky-Geier. 2009. Dynamics of excitable elements with time-delayed coupling. *J. Theor. Biol.* 259:96–100.
10. Berridge, M. J. 1990. Calcium oscillations. *J. Biol. Chem.* 265: 9583–9586.
11. Rooney, T. A., E. J. Sass, and A. P. Thomas. 1989. Characterization of cytosolic calcium oscillations induced by phenylephrine and vasopressin in single Fura-2-loaded hepatocytes. *J. Biol. Chem.* 264:17131–17141.
12. Lechleiter, J., S. Girard, …, D. Clapham. 1991. Spiral calcium wave propagation and annihilation in *Xenopus laevis* oocytes. *Science.* 252:123–126.
13. Rintoul, G. L., and K. G. Baimbridge. 2003. Effects of calcium buffers and calbindin-D28k upon histamine-induced calcium oscillations and calcium waves in HeLa cells. *Cell Calcium.* 34:131–144.
14. Dargan, S. L., B. Schwaller, and I. Parker. 2004. Spatiotemporal patterning of IP3-mediated $Ca^{2+}$ signals in *Xenopus* oocytes by $Ca^{2+}$-binding proteins. *J. Physiol.* 556:447–461.
15. Falcke, M. 2003. Buffers and oscillations in intracellular $Ca^{2+}$ dynamics. *Biophys. J.* 84:28–41.
16. Wagner, J., and J. Keizer. 1994. Effects of rapid buffers on $Ca^{2+}$ oscillations and $Ca^{2+}$ diffusion. *Biophys. J.* 67:447–456.
17. Smith, G. D. 1996. Analytical steady-state solution to the rapid buffering approximation near an open $Ca^{2+}$ channel. *Biophys. J.* 71:3064–3072.
18. Smith, G. D., J. Wagner, and J. Keizer. 1996. Validity of the rapid buffering approximation near a point source of calcium ions. *Biophys. J.* 70:2527–2539.
19. Smith, G., L. Dai, …, A. Sherman. 2001. Asymptotic analysis of buffered calcium diffusion near a point source. *SIAM J. Appl. Math.* 61:1816–1838.
20. Shuai, J., J. E. Pearson, and I. Parker. 2008. Modeling $Ca^{2+}$ feedback on a single inositol 1,4,5-trisphosphate receptor and its modulation by $Ca^{2+}$ buffers. *Biophys. J.* 95:3738–3752.
21. Shuai, J., J. E. Pearson, …, I. Parker. 2007. A kinetic model of single and clustered $IP_3$ receptors in the absence of $Ca^{2+}$ feedback. *Biophys. J.* 93:1151–1162.
22. Swillens, S., G. Dupont, …, P. Champeil. 1999. From calcium blips to calcium puffs: theoretical analysis of the requirements for interchannel communication. *Proc. Natl. Acad. Sci. USA.* 96:13750–13755.
23. Shuai, J. W., and P. Jung. 2003. Optimal ion channel clustering for intracellular calcium signaling. *Proc. Natl. Acad. Sci. USA.* 100:506–510.
24. Shuai, J., D. Yang, …, S. Rüdiger. 2009. An investigation of models of the IPR channel in *Xenopus* oocyte. *Chaos.* 19:037105.
25. De Young, G. W., and J. Keizer. 1992. A single-pool inositol 1,4,5-trisphosphate-receptor-based model for agonist-stimulated oscillations in $Ca^{2+}$ concentration. *Proc. Natl. Acad. Sci. USA.* 89:9895–9899.
26. Nagaiah, C., S. Rüdiger, …, M. Falcke. 2008. Adaptive numerical simulation of intracellular calcium dynamics using domain decomposition methods. *Appl. Numer. Math.* 58:1658.
27. Rüdiger, S., J. W. Shuai, …, M. Falcke. 2007. Hybrid stochastic and deterministic simulations of calcium blips. *Biophys. J.* 93:1847–1857.
28. Shuai, J., H. J. Rose, and I. Parker. 2006. The number and spatial distribution of $IP_3$ receptors underlying calcium puffs in *Xenopus* oocytes. *Biophys. J.* 91:4033–4044.
29. Demuro, A., and I. Parker. 2008. Multi-dimensional resolution of elementary $Ca^{2+}$ signals by simultaneous multi-focal imaging. *Cell Calcium.* 43:367–374.
30. Sneyd, J., and M. Falcke. 2005. Models of the inositol trisphosphate receptor. *Prog. Biophys. Mol. Biol.* 89:207–245.

Biophysical Journal, Volume 99

**Supporting Material**

# Calcium domains around single and clustered IP3 receptors and their modulation by buffers

Sten Ruediger, Chamakuri Nagaiah, Gerald Warnecke, and Jianwei Shuai

# Supporting Material
# Calcium domains around single and clustered $IP_3$ receptors and their modulation by buffers

S. Rüdiger
Institute of Physics,
Humboldt-Universität zu Berlin, Germany,
Ch. Nagaiah
Institute of Mathematics and Scientific Computing,
University of Graz, Austria,
G. Warnecke
Institute for Analysis and Numerics,
Otto-von-Guericke University Magdeburg, Germany
J.W. Shuai
Department of Physics,
and Institute of Theoretical Physics and Astrophysics
Xiamen University, China

# S1. Model equations

## Partial differential equations for the concentration fields (multi-channel simulations)

The calcium concentration in the cytosol is determined by diffusion, transport of calcium through the ER membrane, and binding and unbinding of calcium to buffer molecules. In the cytosol we consider the following types of buffers: exogenous mobile buffer with fast or slow reaction kinetics and a stationary buffer with fast kinetics.

Buffers are assumed to be distributed homogeneously at initial time. Total concentrations of mobile and stationary buffers are denoted by $B_m$ and $B_{imm}$, while the concentrations of corresponding buffer bound to calcium are denoted by $b_m$ and $b_{imm}$, respectively, which are determined by mass-action dynamics:

$$\frac{\partial c}{\partial t} = D\nabla^2 c - k_m^+(B_m - b_m)c + k_m^- b_m - k_{imm}^+(B_{imm} - b_{imm})c + k_{imm}^- b_{imm}, \quad (1)$$

$$\frac{\partial b_m}{\partial t} = D_m\nabla^2 b_m + k_m^+(B_m - b_m)c - k_m^- b_m, \quad (2)$$

$$\frac{\partial b_{imm}}{\partial t} = k_{imm}^+(B_{imm} - b_{imm})c - k_{imm}^- b_{imm}. \quad (3)$$

Here, the $k^\pm$ denote the on and off rates of calcium reacting with the corresponding buffer proteins. Parameters for the mobile and stationary types of buffers used for this work are listed in Tab. S1. The equations are solved in a rectangular box domain bounded on one side by an idealized quadratic membrane patch of $(8+3\times d)$ $\mu$m side length, where $d$ is the distance between the channels. In the $z$-direction, perpendicular to the membrane, we consider a spatial extent of $5$ $\mu$m. All boundary conditions except for $c$ at the ER membrane are no-flux conditions. The boundary condition for $c$ at the membrane models the transport through the membrane,

$$D\partial_z c = -J, \text{ at } z = 0 \quad (4)$$

and comprises three contributions:

$$J = P_c S(\vec{r}, t)(E - c) - P_p \frac{c^2}{K_d^2 + c^2} + P_l(E - c), \quad (5)$$

where $\vec{r} = (x, y, 0)$ denotes the position on the membrane. Calcium moves from the ER to the cytosol through $IP_3$ receptors and by a small leak contribution, which are modeled by terms with coefficients $P_c$ and $P_l$, respectively. In the other direction calcium is resequestered into the ER by pumps ($P_p$). The action of pumps is assumed to be cooperative in calcium and modeled with a quadratic $c$ dependence. $K_d$ is the dissociation constant of the pumps. The first term in Eq. 5 represents the current through the channel, where $P_c$ is adjusted such as to represent a total current of 0.1 pA if the channel is open (in the single-channel simulations, owing to the spherical symmetry of the cytosolic space, we adjusted the current through the channel to 0.2 pA.) We model the source area of a channel by a circle of radius $R_s = 6$ nm (1). The positions of channels in the rectangular box are given by $\vec{X}_{kl} = ((4 + (k + 1/2)d)\,\mu\text{m}, (4 + (l + 1/2)d)\,\mu\text{m}, 0)$, where $k$ and $l$ run from 0 to 2. The channel flux term in Eq. 5 is

controlled by the channel state through the factor $S(\vec{r},t)$, which is defined by:

$$S(\vec{r},t) = \begin{cases} 1, & \text{if there is an open channel } (k,l) \text{ and } \left\|\vec{r} - \vec{X}_{kl}\right\| < R_s, \\ 0, & \text{otherwise.} \end{cases}$$

For a more detailed description of the membrane current modeling we refer to (2). The parameters that we use in the current work are shown in Tables S1 and S2.

# S2. Numerical methods

## S2.1 Single-channel simulations

We here consider a single $IP_3R$ channel that is located in the center of the cytosol space. For simplicity, we ignore the pump dynamics and the leakage flux on the ER membrane and use spherical symmetry around the channel pore. Thus the diffusion of free $Ca^{2+}$ and buffers bound to $Ca^{2+}$ can be described in spherical coordinates with the Laplacian operator

$$\nabla^2 c(r) = \frac{2}{r}\frac{\partial c}{\partial r} + \frac{\partial^2 c}{\partial r^2}. \tag{6}$$

The finite difference method proposed by Smith et al. was used to solve the partial differential equations (3). In order to enhance the computation speed, we further applied a multiple-grid-size method to discretize the cytosolic space (4). The grid size is 5 nm near the channel pore and increases to 80 nm far from the channel. At the boundary of the system, the concentrations of all species are held constant at their resting levels.

In our simulations we put the $Ca^{2+}$ binding sites of the $IP_3R$ at the channel pore, at which the free $Ca^{2+}$ concentration typically reaches about 370 μM during the channel open period. It should be noted that with a larger flux source area (such as with a radius of 6 nm as used for the multi-channel simulations) or with a larger distance of the binding site from the channel pore, the binding calcium concentration can be decreased to around 100 $\mu$M. However, this modification will not alter our main conclusions about the buffer effect since significant binding processes are governed by domain calcium concentrations as shown in the main text.

In the single channel model, the current is 0.2 pA. As a fact, the calcium diffusion in the full three dimensional space for a single channel with 0.2 pA is equivalent to the diffusion in a half space for the single channel with current 0.1 pA. In this case, the same geometry and channel current are used for both single channel system and cluster system.

## S2.2 Multi-channel setup

Our numerical method consists of coupled solvers for the deterministic set of PDEs and the stochastic equations. In view of the multiple scales in length and time we employ a conforming finite element method for the spatial discretization and an adaptive linear implicit time-stepping for the deterministic part. The stochastic solver is based on the Gillespie method (5), which is adaptive in the sense that its time step follows the evolution of transition probabilities. A complication arises since the usual Gillespie method solves stochastic processes where the transition rates are constant during subsequent transitions.

However, for channels with $Ca^{2+}$ as carrier the rates may change rapidly due to channel openings and closings. This problem was solved by devising the hybrid method described in (2), where we introduced and tested the hybrid method for a single channel system—here the obvious generalization to multi-channel systems will be used.

We discretized the spatial domain by linear finite elements (6). The attractive feature of the method is its ability to effectively handle complex geometries. For our simulations of release from clustered channels we employ a grid with a very fine resolution in the channel area. There the grid length is around 0.3 nm. With increasing distance from the channel the grid is coarsened up to 1600 nm.

## S2.3 Stochastic model of channel gating

To incorporate the open/close dynamics of a single or multiple $IP_3$Rs we adopt the 9-state model for the gating of subunits (7), which is based on the DeYoung-Keizer model (8, 9). According to the DeYoung-Keizer model, an $IP_3$R consists of four identical subunits. There are three binding sites on each subunit: An activating site for $Ca^{2+}$, an inhibiting $Ca^{2+}$ site, and an $IP_3$ binding site. The three binding sites allow for 8 different states $X_{ijk}$ of each subunit. The index $i$ indicates the state of the $IP_3$ site, $j$ the one of the activating $Ca^{2+}$ site and $k$ the state of the inhibiting $Ca^{2+}$ site. An index is 1 if a $Ca^{2+}$ ion or $IP_3$ is bound and 0 if not. Rates of transitions involving binding of a molecule are proportional to the concentration of the respective molecule.

A further transition from $X_{110}$ (the state with $IP_3$ bound and activating $Ca^{2+}$ bound) to a state denoted by $X_{ACT}$ is introduced (7). It represents a conformational change of the subunit related to the channel opening. The on- and off-rates of the transition from $X_{110}$ to $X_{ACT}$ are $a_0$ and $b_0$, respectively. We assume that the channel is open if at least three of the subunits are in the $X_{ACT}$ state. The parameters of the nine-state gating model are listed in Tab. S2, where we follow the notion introduced in (7).

We associate nine stochastic variables $X_{000}(i)$, $X_{001}(i)$, ..., $X_{ACT}(i)$ to each channel $i$. These variables count the numbers of subunits of channel $i$ that are in the respective state. That is, each variable can take on values from 0 to 4, while the sum of all nine variables for each channel must equal 4. The $Ca^{2+}$ concentration for the activation and inhibition processes are evaluated at the channel center position. In the multi-channel simulations this value for an open channel reaches 110 $\mu$M, in the single channel simulations it is around 370 $\mu$M. This difference is due to the different grid distances used in these two simulation schemes. To be specific, the radius of the flux source is 6 nm for the 9 channel simulations and 2.5 nm for the single channel simulations.

## S2.4 Two-buffer simulations for multi-channel setup

Since the computational effort of our simulations increases with the number of buffers, we decided to use a simplification in these multi-channel calculations. First, using the finite-element code, we chose a relatively large distance of the channels of 120 nm. This allowed us to increase the pore size to a radius of 24 nm, which, together with a corresponding reduction of ion current per unit area, relaxes calcium concentration gradients and thus permits a coarser numerical grid. While for the small-pore method 114000 grid point are needed, we now only need 34000 grid points using the approximation method. To account for the large local calcium concentration during channel opening, we set the concentration to a fixed value of 110 µM whenever the particular channel is open. We estimated this value to be close to a universal concentration at the channel mouth in the open state, independent on conditions such as

channel distance or buffers.

# S3. Additional results

## S3.1 Single channel simulations

Different types of exogenous mobile buffers, including various calcium fluorescent dye buffers, are available and applied for experimental study in order to achieve the best resolution for different research purposes. BAPTA and EGTA represent two types of buffers with either fast or slow calcium binding/unbinding rates.

We studied the effects of EGTA and BAPTA on single channel simulations in the presence of stationary buffer (Fig. S1). The immobile buffer is fixed at 800 $\mu$M in the system. A detailed discussion of Fig. S1 is given in the main text. We also studied the effect of changing the diffusion coefficient on single channel dynamics for fast calcium binding/unbinding buffers. Fig. S2 shows the single channel dynamics as a function of diffusion coefficient with mobile buffer concentration 500 $\mu$M. With small diffusion coefficient, mobile buffer is more like an immobile buffer, resulting in a large open probability for single channel dynamics due to the largely slow decay of free $Ca^{2+}$ right after channel closed. Increasing the diffusion coefficient of the mobile buffer will increase the shuttle effect for the mobile buffer to remove the free calcium ions away from the channel pore domain right after the channel closed. Thus, the reopening probability for the closed channel becomes smaller with a larger diffusion coefficient of the mobile buffer, resulting in a longer mean close time and a larger open probability of the single channel (Fig. S2).

We finally discuss the effect of changing the $IP_3$ concentration under different buffer configurations. As shown in Fig. S3, with increasing $IP_3$ concentrations, generally the open probability increases, the mean close time decreases, and the mean open time increases slightly. The data shows that the largest open probability is obtained for immobile buffer, while the additional presence of mobile buffer reduces the open probability compared to the immobile buffer case. We thus conclude that the results discussed in the main text for the dependence of open probability on buffer type and concentration are generally valid independent on $IP_3$ concentration.

## S3.2 Multi-channel simulations

Fig. S4 shows typical spatial distributions of free calcium and $Ca^{2+}$ bound buffer at the membrane in a 600 nm $\times$ 600 nm cluster area ($d = 120$ nm) during release for different types of buffer. [$Ca^{2+}$] is plotted in logarithmical scale while buffer concentration is plotted in linear scale. In all four considered cases (control (a), and either 800 μM immobile buffer (b), fast mobile buffer (c), or slow mobile buffer (d)) open channels are characterized by a free calcium concentration of around 100 $\mu$M, while the calcium distribution in the cluster area and the distribution of calcium bound buffer strongly depends on the type of buffer.

# References

1. Thul, R., and M. Falcke, 2004. Release currents of $IP_3$ receptor channel clusters and concentration profiles. *Biophys.J.* 86:2660–2673.

2. Rüdiger, S., J. Shuai, W. Huisinga, C. Nagaiah, G. Warnecke, I. Parker, and M. Falcke, 2007. Hybrid Stochastic and Deterministic Simulations of Calcium Blips. *Biophys. J.* 93:1847–1857.

3. Smith, G., J. Wagner, and J. Keizer, 1996. Validity of the rapid buffer approximation near a point source of calcium ions. *Biophys.J.* 70:2527–2539.

4. Shuai, J., J. Pearson, and I. Parker, 2008. Modeling $Ca^{2+}$ Feedback on a Single Inositol 1, 4, 5-Trisphosphate Receptor and Its Modulation by $Ca^{2+}$ Buffers. *Biophysical Journal* 95:3738.

5. Gillespie, D. T., 1977. Exact Stochastic Simulation of Coupled Chemical Reactions. *J. Phys. Chem.* 8:2340.

6. Nagaiah, C., S. Rüdiger, G. Warnecke, and M. Falcke, 2008. Adaptive numerical simulation of intracellular calcium dynamics using domain decomposition methods. *Applied Numerical Mathematics* 58:1658.

7. Shuai, J., J. E. Pearson, J. K. Foskett, D. D. Mak, and I. Parker, 2007. A Kinetic Model of Single and Clustered $IP_3$ receptors in the Absence of Ca2+ Feedback. *Biophys. J.* 93:1151–1162.

8. DeYoung, G., and J. Keizer, 1992. A single-pool inositol 1,4,5-trisphosphate-receptor-based model for agonist-stimulated oscillations in $Ca^{2+}$ concentration. *Proc.Natl.Acad.Sci USA* 89:9895–9899.

9. Keizer, J., and G. DeYoung, 1994. Simplification of a realistic model of $IP_3$-induced $Ca^{2+}$ oscillations. *J.theor.Biol.* 166:431–442.

10. Dargan, S., and I. Parker, 2003. Buffer kinetics shape the spatiotemporal patterns of $IP_3$-evoked $Ca^{2+}$ signals. *J.Physiol.* 553:775–788.

11. Smith, I., and I. Parker, 2009. Imaging the quantal substructure of single IP3R channel activity during Ca2+ puffs in intact mammalian cells. *Proceedings of the National Academy of Sciences* 106:6404.

12. Allbritton, N., T. Meyer, and L. Sryer, 1992. Range of messenger action of Calcium ion and inositol 1,4,5 trisphosphate. *Science* 258:1812–1815.

| **Buffer** | **parameter** | **value** | **unit** |
|---|---|---|---|
| slow buffer (EGTA) | | | |
| | $k_m^+$ | 6 (10) | $(\mu\text{M s})^{-1}$ |
| | $k_m^-$ | 1 (10) | $\text{s}^{-1}$ |
| fast buffer (BAPTA) | | | |
| | $k_m^+$ | 600 (10) | $(\mu\text{M s})^{-1}$ |
| | $k_m^-$ | 100 (10) | $\text{s}^{-1}$ |
| stationary buffer | | | |
| | $k_{imm}^+$ | 50 (1) | $(\mu\text{M s})^{-1}$ |
| | $k_{imm}^-$ | 100 (1) | $\text{s}^{-1}$ |

Table S1. List of buffer kinetic parameters. Numbers in brackets denote reference publications for the given values.

| Parameter | symbol | value | unit |
|---|---|---|---|
| **geometry** | | | |
| membrane length | | $> 8$ | $\mu$m |
| channels per cluster | | 9 (11) | |
| channel radius | $R_s$ | 6 (1) | nm |
| **diffusion coefficients** | | | |
| free $Ca^{2+}$ | $D_c$ | 220 (12) | $\mu m^2 s^{-1}$ |
| mobile buffer | $D_m$ | 95 (3) | $\mu m^2 s^{-1}$ |
| **rest concentration** | | | |
| free $Ca^{2+}$ | $c_0$ | 0.05 | $\mu$M |
| **membrane transport parameters** | | | |
| channel flux coefficient | $P_c$ | $6.32 \times 10^6$ (2) | nm $s^{-1}$ |
| pump flux coefficient | $P_p$ | 40000 (1) | nm $\mu$M $s^{-1}$ |
| **9-state model** | | | |
| | $a_0$ | 540 | $s^{-1}$ |
| | $b_0$ | 80 | $s^{-1}$ |
| $IP_3$-binding | | | |
| | $a_1$ | 60 | $(\mu M\ s)^{-1}$ |
| | $a_3$ | 5 | $(\mu M\ s)^{-1}$ |
| | $d_1$ | 0.0036 | $\mu$M |
| | $d_3$ | 0.8 | $\mu$M |
| activating $Ca^{2+}$ | | | |
| | $a_5$ | 30 | $(\mu M\ s)^{-1}$ |
| | $d_5$ | 0.8 | $\mu$M |
| inhibiting $Ca^{2+}$ | | | |
| | $a_2$ | 0.04 | $(\mu M\ s)^{-1}$ |
| | $a_4$ | 0.5 | $(\mu M\ s)^{-1}$ |
| | $d_2$ | 16 | $\mu$M |
| | $d_4$ | 0.072 | $\mu$M |
| pump—dissociation coefficient | $K_d$ | 0.2 (1) | $\mu$M |
| $Ca^{2+}$ concentration in ER | $ER_{const}$ | 700 (1) | $\mu$M |
| stimulating $IP_3$ concentration | | 0.2, 1.0 | $\mu$M |

Table S2. List of parameters used for our model. $P_p$ and $P_l$ have been chosen to yield a rest concentration of $c_0 = 0.05$ µM . The on-rates $a_i$, off-rates $b_i$ and the dissociation constants $d_i$ are related by $d_i = b_i/a_i$.

# Figure Legends

**Figure S1.**

The blip characteristics as a function of mobile concentration in the presence of 800 μM immobile buffer. (A) is the mean close time, (B) the mean open time, and (C) the open probability. In the figure, the stars are for BAPTA and circles for EGTA.

**Figure S2.**

The blip characteristics as a function of diffusion coefficient of fast buffer in the presence of 800 μM immobile buffer. (A) is the mean close time, (B) the mean open time, and (C) the open probability. Here the fast mobile buffer concentration is 500 $\mu$M.

**Figure S3.**

The blip characteristics as a function of $IP_3$ concentration. We compare four scenarios: no buffer, 800 μM immobile buffer, 800 μM immobile buffer and 500 μM BAPTA, 800 μM immobile buffer and 500 μM EGTA. (A) is the mean close time, (B) the mean open time, and (C) the open probability.

**Figure S4.**

The free calcium concentration (red) and the concentration of $Ca^{2+}$ bound buffer (blue) in the central cluster area of side length 600 nm: without buffer (A), with immobile buffer (B), fast mobile buffer (C), and slow mobile buffer (D). The scales are logarithmic for calcium and linear for calcium bound buffer. Note that in C, $[Ca^{2+}]$ is practically at rest level at the location of closed channels.

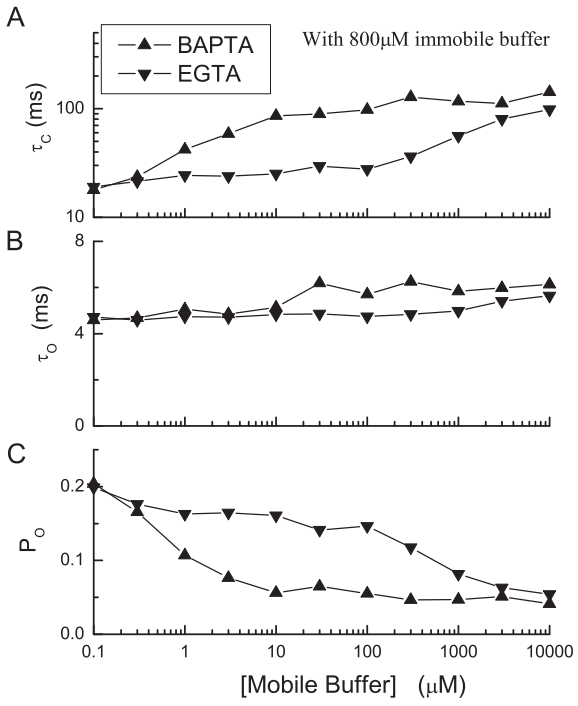
A
BAPTA
EGTA
With 800μM immobile buffer
τC (ms)
100
10
B
8
τO (ms)
4
0
C
0.2
PO
0.1
0.0
0.1
1
10
100
1000
10000
[Mobile Buffer] (μM)

Figure S1:

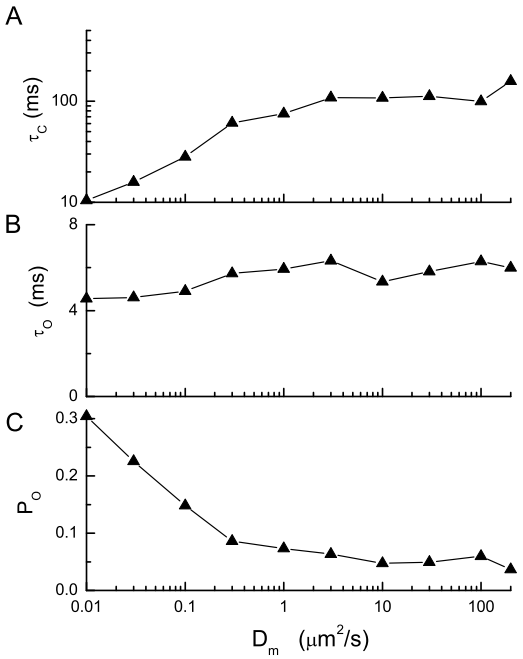
A
B
C
$\tau_C$ (ms)
100
10
$\tau_O$ (ms)
8
4
0
$P_O$
0.3
0.2
0.1
0.0
0.01
0.1
1
10
100
$D_m$ ($\mu m^2$/s)

Figure S2:

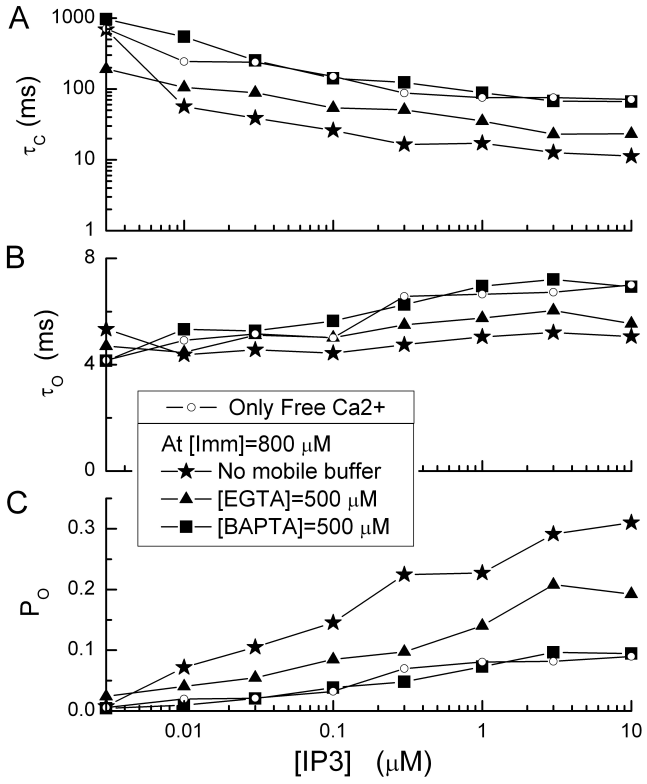
A
1000
100
10
1
τC (ms)
B
8
4
0
τO (ms)
Only Free Ca2+
At [Imm]=800 μM
No mobile buffer
[EGTA]=500 μM
[BAPTA]=500 μM
C
0.3
0.2
0.1
0.0
PO
0.01
0.1
1
10
[IP3] (μM)

Figure S3:

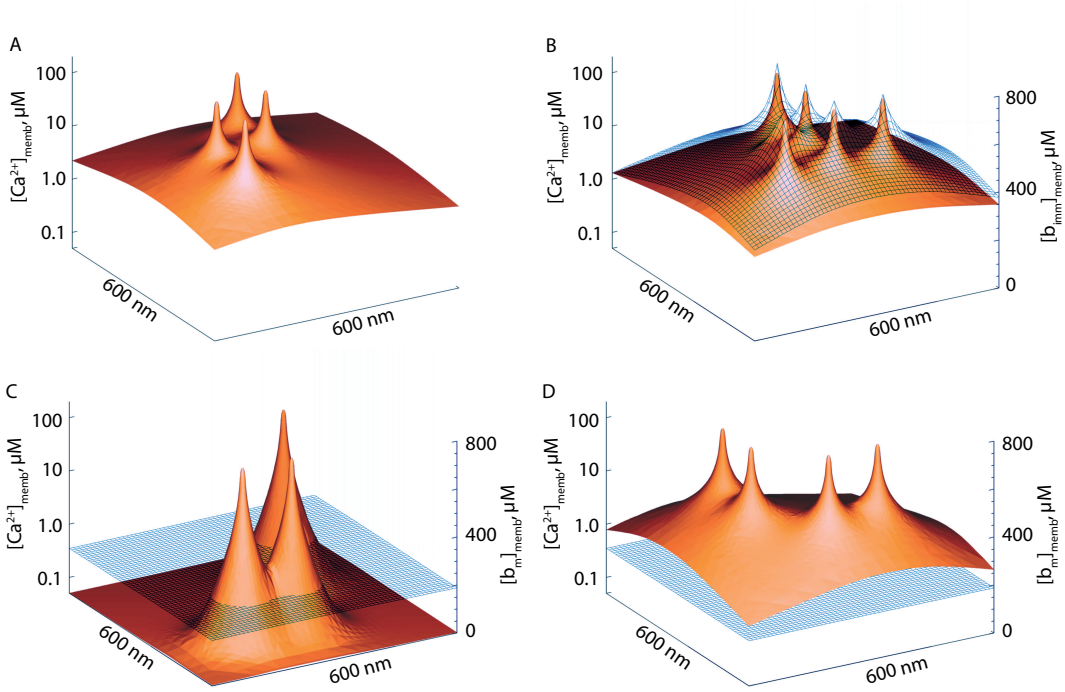
A
B
C
D
100
10
1.0
0.1
800
400
0
600 nm
600 nm
[Ca2+]membr, μM
[bimm]membr, μM
[bm]membr, μM

Figure S4: